Titania–hydroxyapatite nanocomposite coatings support human mesenchymal stem cells osteogenic differentiation

Dimitrievska, Sashka; Bureau, Martin N.; Antoniu, John; Mwale, Fackson; Petit, Alain; Lima, Rogerio S.; Marple, Basil R.

Publisher's version / Version de l'éditeur:
https://doi.org/10.1002/jbm.a.32964
Journal of Biomedical Materials Research Part A, 2011-06-23

Titania–hydroxyapatite nanocomposite coatings support human mesenchymal stem cells osteogenic differentiation

Sashka Dimitrievska,[1] Martin N. Bureau,[1] John Antoniou,[2] Fackson Mwale,[2] Alain Petit,[2] Rogerio S. Lima,[1] Basil R. Marple[1]

[1]National Research Council Canada – Industrial Materials Institute, 75 boul de Mortagne, Boucherville, QC J4B 6Y4, Canada
[2]Division of Orthopaedic Surgery, McGill University, Lady Davis Institute for Medical Research, SMBD – Jewish General Hospital, 3755 Chemin de la Côte Ste-Catherine, Montreal, QC H3T 1E2, Canada

Received 8 February 2010; revised 13 July 2010; accepted 30 July 2010
Published online in Wiley Online Library (wileyonlinelibrary.com). DOI: 10.1002/jbm.a.32964

Abstract: In addition to mechanical and chemical stability, the third design goal of the ideal bone-implant coating is the ability to support osteogenic differentiation of mesenchymal stem cells (MSCs). Plasma-sprayed TiO_2-based bone-implant coatings exhibit excellent long-term mechanical properties, but their applications in bone implants are limited by their bioinertness. We have successfully produced a TiO_2 nanostructured (grain size $<$50 nm) based coating charged with 10% wt hydroxyapatite (TiO_2–HA) sprayed by high-velocity oxy-fuel. On Ti64 substrates, the novel TiO_2–HA coating bond 153$\times$ stronger and has a cohesive strength 4$\times$ higher than HA coatings. The HA micro- and nano-sized particles covering the TiO_2–HA coating surface are chemically bound to the TiO_2 coating matrix, producing chemically stable coatings under high mechanical solicitations. In this study, we elucidated the TiO_2–HA nanocomposite coating surface chemistry, and *in vitro* osteoinductive potential by culturing human MSCs (hMSCs) in basal and in osteogenic medium (hMSC-ob). We assessed the following hMSCs and hMSC-ob parameters over a 3-week period: (i) proliferation; (ii) cytoskeleton organization and cell–substrate adhesion; (iii) coating–cellular interaction morphology and growth; and (iv) cellular mineralization. The TiO_2–HA nanocomposite coatings demonstrated 3$\times$ higher hydrophilicity than HA coatings, a TiO_2-nanostructured surface in addition to the chemically bound HA micron- and nano-sized rod to the surface. hMSCs and hMSC-ob demonstrated increased proliferation and osteoblastic differentiation on the nanostructured TiO_2–HA coatings, suggesting the TiO_2–HA coatings nanostructure surface properties induce osteogenic differentiation of hMSC and support hMSC-ob osteogenic potential better than our current golden standard HA coating. Published 2011 Wiley Periodicals, Inc. J Biomed Mater Res Part A: 00A: 000–000, 2011.

Key Words: mesenchymal stem cells (MSCs), osteogenic differentiation *in vitro*, nanostructured titania–hydroxyapatite (TiO_2–HA) coatings

INTRODUCTION

Bone is characterized by a lifelong growth, regeneration, and remodelling potential. This is largely due to the directed differentiation of mesenchymal cells into osteogenic cells, a process subject to exquisite regulation and complex interplay by a variety of hormones, differentiation factors, and environmental cues present within the bone matrix.[1,2] However, acute osteoporotic as well as badly damaged bones fail to sufficiently regenerate and are often replaced with titanium (Ti) based bone implants. The hydroxyapatite (HA) thermally sprayed coating of Ti, advocated to improve Ti bioactivity, is clinically plagued by low crystallinity, poor bonding strength, degradation during the thermal spray processing[3,4] possibly leading to implantation driven dissolution,[5] and possible late delamination of the coating with formation of particulate debris and third-body wear.[5] Although a comprehensive review of the literature supports the bone directed HA bioactivity and the use of HA-coated cementless femoral stems, some authors have reported that HA-induced bioactivity is controversial because of the drawbacks of HA's poor mechanical properties.[5] To preserve HA bioactivity a coating with higher bond and cohesive strengths as well as chemical stability under high mechanical solicitations is needed.

Since the early 1990s, there has been significant research to establish the correct biological stimuli required to obtain osteoblasts from human mesenchymal stem cells (hMSC) by the use of supplemented media.[1,6,7] More recently, researchers have focused on 2D substrate-induced hMSC osteogenesis and substrate-induced bioactivity.[2,7–11] However, the current lack of knowledge about substrate characteristics such as surface chemistry and topography control over hMSC behaviour and differentiation has largely restricted hMSC osteogenic differentiation to biological intervention in the form of growth factors and cytokines. Despite current efforts, the optimal bone implant coatings capable of influencing and accommodating the growth and osteogenic differentiation of hMSCs are yet to be identified.

Recently, thermally sprayed coatings produced via high-velocity oxy-fuel (HVOF) from blends of nanostructured TiO_2 and HA powders were developed (TiO_2–HA). These novel TiO_2–HA nanocomposite coatings, containing 10% (wt)

Correspondence to: S. Dimitrievska; e-mail: sashka.dimitrievska@yale.edu

HA, exhibit at least 3× higher bond strength and 4× higher cohesive strength values on Ti–6Al–4V (Ti64) substrates than HA coatings.[4] In addition to their mechanical properties, the TiO_2–HA nanocomposite coatings have been engineered to exhibit a surface nanotopography with distinct repeating nanoscopique zones[3] originating from the TiO_2 agglomerated clusters. TiO_2–HA coatings strong adhesion and high stability on Ti64 have resulted significant research activity,[12–17] without any commercial scale implant production. Because of the large sizes of femoral implants, plasma spray is the only commercially used coating technique,[17] although literature explored TiO_2–HA coatings are also produced by sol–gel,[14,18] IonTite,[13] and electron beam (e-beam)[16] techniques. Regardless of the production technique, TiO_2–HA coatings demonstrate promising biological responses in increasing bone regeneration, largely increased when producing nanophase/nanocrystaline coatings.[4,13]

In our previous studies, we demonstrated greater bone contact surface in rabbit femurs *in vivo*[3,19] on pure nanostructured TiO_2-coated implants when compared with industry-used air plasma-sprayed (APS) HA coatings. In an attempt to further increase the coating bioactivity by incorporating HA chemistry-related bioactivity,[4] we added 10% (wt) HA from nanostructured HA starting powders. In the present study, we sought to characterize the HA-enhanced TiO_2-nanostructured coatings surface chemistry and bioactivity with hMSC from total hip revision patients. The results were compared with a surface which is commonly used for hip prosthesis coatings (i.e., standard FDA-approved single-phase HA coating). It is our belief that HVOF sprayed TiO_2–HA nanocomposites coatings hydrophilicity, surface nanostructure, and chemically bound micro-sized HA rods would offer an improved 2D substrate to hMSC adhesion, growth and osteoblastic differentiation.

MATERIALS AND METHODS

Preparation of nanocomposite coatings

Our studies are based on three types of coatings: in addition to the nanocomposite TiO_2–HA candidate coating, two reference coatings, the APS-sprayed HA and HVOF-sprayed TiO_2 coatings, were also deposited on grit-blasted Ti64 alloy substrates. The TiO_2 and TiO_2–HA nanocomposite powders were thermally sprayed via the HVOF technique using an oxy-propylene based HVOF torch (Diamond Jet 2700-hybrid, Sulzer Metco, Westbury, NY). More information about powder composition, powder mixture, spraying, and coating microstructure can be found elsewhere.[3] The HA powder was thermally sprayed using an APS torch (SG100, Praxair, Concord, NH) using only argon (Ar) as plasma gas, reproducing the conditions and coating previously described.[20] Particle characterization was performed to evaluate in-flight particle properties. For this purpose, an in-flight diagnostic tool (DPV 2000, Tecnar Automation, Saint-Bruno, QC) was used. This system uses infrared pyrometry to perform the in-flight diagnostics on 5000 sprayed particles. The measurements were performed from the centerline of the spray jet at the standoff distance for coating deposition, which was 20 cm for HVOF and 7.5 cm for APS. The average surface temperature and velocity values for the TiO_2 particles were 1881 ± 162°C and 686 ± 93 m/s. For the TiO_2–HA nanocomposite particles they were 1875 ± 162°C and 651 ± 88 m/s, respectively.[21] The HA particles were deposited at particle temperature and velocity of 2659 ± 234°C and 189 ± 19 m/s, respectively. During the spraying process, the substrate temperature was recorded using a pyrometer. A cooling system (air jets) was used to maintain the coating temperature below 170°C for all sprayed coatings. The coatings were cleaned by two-step ultrasonification involving 99.9% ethanol and 98.9% acetone for 10 min cycles each. The samples were then wrapped in plastic sterilization pouches and sterilized using pure ethylene oxide (EtO). EtO sterilization was performed in SteriVac® with a 4-h cycle followed by 24 h sterile aeration to remove residual EtO.

Surface characterization of coatings

Scanning electron microscopy (S4700, Hitachi, Tokyo, Japan) coupled with an energy-dispersive X-ray (EDX) was used to characterize the interdiffusion among the elements of TiO_2 and HA in the TiO_2–HA nanocomposite. SEM was used to characterize the surface morphology of the coatings and the dispersion of HA phase within the TiO_2 phase. The average surface roughness (R_a) of the samples in the micrometer range was measured using a mechanical stylus-type roughness tester (Surftest 301, Mitutoyo, Kanagawa, Japan). The R_a is the average height of the asperities of a surface measured from a mean line. It is given by the formula $R_a = (1/L)\int_{x=0}^{x=L} |y(x)|dx$, where y is the deviation of the surface profile from the mean line and L is the measured length. The average nanometer-range surface roughness was measured by two parameters R_a and S_a using a confocal imaging profiler (Eclipse L150 Sensofar, Nikon, Tokyo, Japan), with a ×50/0.80 numerical aperture and an extra-long working distance dry objective (Nikon). S_a is the average of the distances of the surface points of a mean plane. It is given by the formula $S_a = (1/(N_xN_y))\sum_{i=1}^{N_y}\sum_{j=1}^{N_x}|Z(x_j,y_i)|$, where N_x and N_y are the number of data points in the x and y directions and $Z(x, y)$ is the height value of the roughness surface in point (x, y). By using confocal microscopy the R_a value can also be determined by analyzing a single line measured over an area. Images were captured by a CCD camera (Nikon) and reconstructed with a computer software program (Confocal Imaging Profiler, Mountain Lakes, NJ). Average surface nano-roughness was quantitatively expressed as a numerical value (in nm). The static water contact angles of the coatings were measured at 24°C, using the sessile drop method with a 3-μL water droplet, in a telescopic goniometer (Rame-Hart model 100-00-(230), Rame-Hart, Inc., Mountain Lakes, NJ). The telescope with a magnification power of 23× was equipped with a protractor of 1° graduation. For each angle reported, three measurements from different surface locations were averaged. The angle reported was accurate to within ±3°.

Isolation and culture of human MSCs

Bone marrow samples were obtained from 15 mL aspirates from the intramedullary canal of three osteoarthritis

patients undergoing total hip replacement surgery (one woman and two men, aged 52–76 years). This research received the approval of the Research Ethics Committee of the Jewish General Hospital (Montreal, QC) and of the ethics standards of the National Research Council of Canada. Primary cultures of bone marrow cells were established as previously described.[22] In brief, each aspirate was diluted 1:1 with Dulbecco's modified Eagle medium (DMEM) and layered over 1:1 Ficoll (Ficoll-Paque Plus, GE Healthcare Bio-Sciences, Baie-d'Urfe, QC). After centrifugation at 900*g* for 30 min, the mononuclear cell layer was removed from the interface, washed with DMEM, and resuspended in DMEM supplemented with 10% fetal bovine serum (FBS; Hyclone, Logan, UT), 100 units/mL penicillin, 100 mg/mL streptomycin, and 2 m*M* L-glutamine. The cells were plated in 20 mL of medium in a 176 cm^2 culture dish and incubated at 37°C in a 5% CO_2 humidified atmosphere. After 72 h, nonadherent cells were discarded and adherent cells were thoroughly washed twice with DMEM. Thereafter, the cells were expanded as previously described.[22]

Osteogenic differentiation was induced by treating the second passage hMSC with an osteogenic (OS) cocktail of 100 n*M* dexamethasone, 10 m*M* β-glycerolphosphate, and 50 μ*M* ascorbic acid-2-phosphate (Sigma-Aldrich, Oakville, ON) added to the complete DMEM medium.[11] After 6 days of culture with the OS cocktail, Von Kossa staining and alkaline phosphatase (ALP) measurements were done to confirm the differentiation into hMSC-derived osteoblasts, designated as hMSC-ob. hMSC-ob were incubated at 37°C in a 5% CO_2 humidified atmosphere with medium changes every 3 days.

Culture-expanded hMSC and hMSC-ob were trypsinized, counted and seeded separately into EtO sterilized TiO_2, HA, and TiO_2–HA coated scaffolds (13 × 13 × 0.5 mm) at a density of 2×10^4 cells/cm^2. hMSC-seeded TiO_2–HA coatings were continuously cultured in corresponding medium supplemented with 10% FBS, 100 U/mL penicillin, and 100 μg/mL streptomycin described above. hMSC-ob seeded onto TiO_2–HA coated pucks were continuously cultured in DMEM supplemented with 100 n*M* dexamethasone, 10 m*M* β-glycerolphosphate, and 50 μ*M* ascorbic acid-2-phosphate as described above. All cultures were incubated in corresponding medium for up to 21 days. Uncoated Ti64 and tissue culture plate (TCP) seeded in the same manner as the test samples were used as a reference and negative control respectively.

Characterization of cell adhesion and proliferation

Cell adhesion on the different coatings was evaluated at 2 and 6 h after plating. Nonadherent cells were washed with phosphate-buffered saline (PBS) prior to cell activity measurement. Cell proliferation was measured up to 21 days of culture. The metabolic activity was used as an indication of cell number and was monitored using the Alamar Blue assay according to the manufacturer (Biosource, Nivelles, Belgium). The cells were also stained with Trypan Blue (Sigma-Aldrich) and counted using a hemoacytometer. Results were expressed as the mean ± standard deviation. The data were analyzed by using one-way analysis of variance (ANOVA) and post hoc assessment of differences between samples were performed using the Bonferoni's multiple test at the confidence level of 95% ($p < 0.05$).

Osteoblast differentiation

ALP activity, the driver of bone matrix mineralization, was determined in the hMSC and hMSC-ob lysates at 1, 7, and 21 days using a commercially available kit (AnaSpec, San Jose, CA) in accordance with the provided instructions. In brief, the measurements were performed using 100 μL supernatants to which 100 μL of *p*-nitrophenolphosphate dye were added. Absorbance was subsequently measured at 410 nm. Osteocalcin (OC) expression, which is associated with mineral deposition, was determined in the cell lysates using a commercially available ELISA kit (Biomedical Technologies, Stoughton, MA) in accordance with the provided instructions. Experiments were performed in triplicate for each condition with the cells from the three (3) different patients. Data were represented as the mean ± standard deviation (SD). Statistical difference was analysed using one-way analysis of variance (ANOVA) and p values <0.05 were considered significant.

Mineralization

Mineralization was visualized using calcein staining (MP Biomedicals, Solon, OH) of the hMSC and hMSC-ob after 14 days in culture. Staining was performed by incubating at 5 μg/mL calcein to cell cultures for 24 h at 37°C. Cells were then washed three times in PBS with agitation to reduce nonspecific calcein stain and fixed with 3.7% formaldehyde in PBS for 10 min. Cells were washed again two times with PBS and treated with 1% Triton X-100 in PBS for 5 min and 1% BSA for 10 min. After rinsing three times with PBS, cells were mounted on glass slides using Vectashield (Vector, Burlingame, CA) and examined with a Cell Observer System (Carl Zeiss, Berlin, Germany).

Mineralization was also directly evaluated through the complementary semi-quantitative alizarin red staining (ARS). ARS is a common histochemical technique used to detect calcium deposits in mineralized tissues and *in vitro* cell cultures. In brief, cells were rinsed with PBS, fixed with ice-cold 70% ethanol for 1 h, washed once with H_2O, and stained for 10 min with 40 m*M* ASR solution (pH 4.2) at room temperature. Cells were rinsed five times for 15 min with H_2O and PBS in alternation to reduce nonspecific ARS stain. Stained cultures were then photographed with a Nikon camera. The semi-quantification of the ASR staining was determined by measuring the absorbance at 570 nm of the de-stained cultures (using 10% (w/v) cetylpyridinium chloride (CPC) in 10 m*M* sodium phosphate, pH 7.0, for 15 min at room temperature). The results were normalized to protein content.

Cytoskeleton organization

The structural cytoskeleton organization of the cells on the various coatings was assessed by the use of two different fluorescent dyes. The first one, F-actin, revealed the general cellular cytoskeletal organization, whereas the second one,

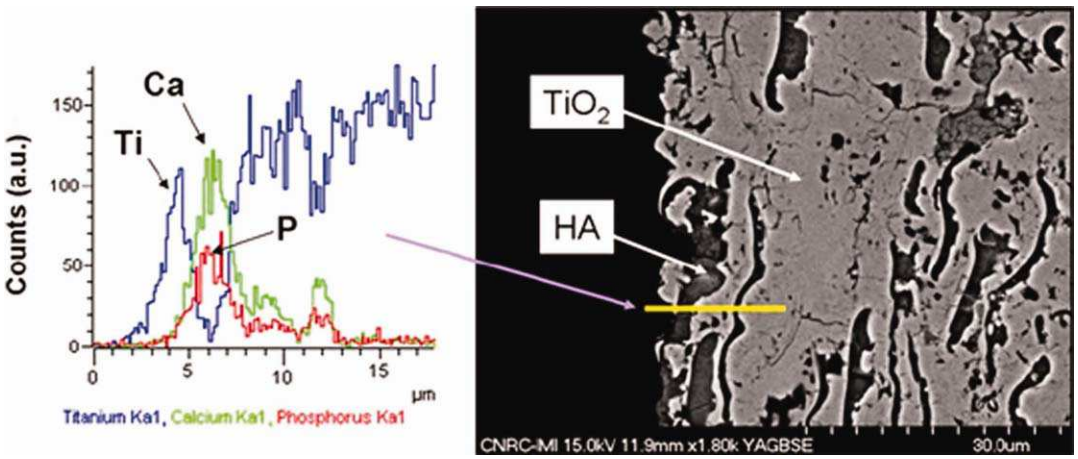

FIGURE 1. Chemical characterization of TiO_2 interaction with HA via energy-dispersive X-ray (EDX) line scan analysis of TiO_2–HA coatings cross-section at the coating elemental interfacial region upper layers is shown. The left-hand side graph is the EDX line scan, and the right-hand side micrograph is the SEM of the TiO_2–HA coatings cross-section. [Color figure can be viewed in the online issue, which is available at wileyonlinelibrary.com.]

propidium iodide (PI), stained specifically the nuclei. In brief, cells were rinsed twice with PBS, fixed in 3.7% methanol-free formaldehyde (Sigma-Aldrich), and permeabilized in 0.1% buffered Triton X-100 (Sigma-Aldrich). Nonspecific binding sites were blocked with 1 g/mL RNase in 1% (w/v) bovine serum albumin (BSA) (Sigma-Aldrich) for 1 h. Cell cytoskeletal F-actin was visualized by treating the cells with 5 U/mL Alexa Fluor 488 phalloidin (Molecular Probes, Burlington, ON) for 1 h. Cell nuclei were then counterstained with PI (Molecular Probes) for 20 min. To visualize focal adhesion and filamentous orientation, cells were also stained for cytoskeletal actin together with vinculin using anti-vinculin (1:100; clone 7F9, Chemicon, Temecula, CA) primary antibodies in 2% BSA/ Dulbecco's phosphate buffered saline (DPBS), (Sigma-Aldrich) for 40 min at room temperature. Revelation was obtained using FITC-labeled anti-rabbit IG antibody (1:200 in 2% BSA/DPBS) for 60 min at RT. Actin filaments were revealed by TRITC-conjugated phalloidin

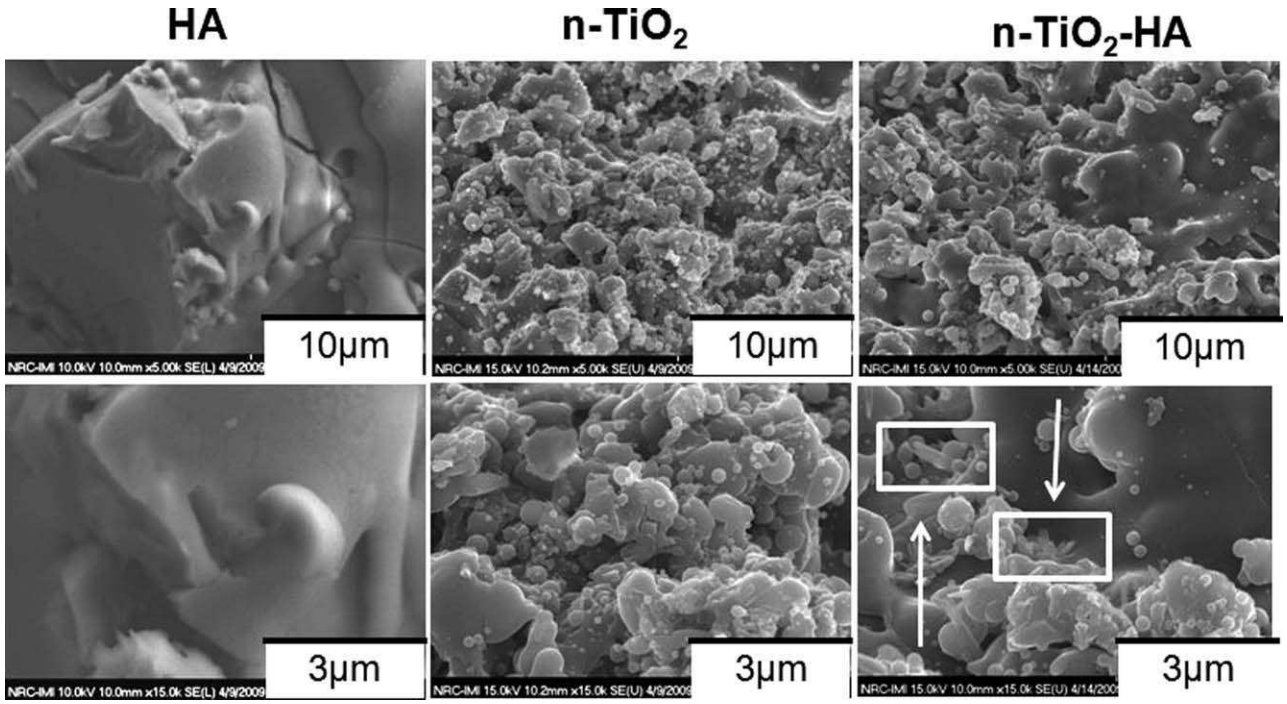

FIGURE 2. Surface morphological characterization of the TiO_2–HA nanocomposite. SEM picture of the reference HA coatings showing the smooth HA surface at nanoscale level, on the left. SEM picture of the reference TiO_2 coatings with a higher magnification picture showing the formation of nano-spherical crystallites on the coating surface, in the middle. SEM picture of the TiO_2–HA nanocomposite coating with higher magnification showing the formation of HA rod-like crystallites and the typical formation of nano-spherical TiO_2 crystallites, to the right.

TABLE I. Physicochemical Characterization of the Pure TiO_2, TiO_2–HA Nanocomposite and Reference HA Coatings

Coating	Micro-roughness R_a (μm)	Nano-roughness R_a (nm)	Nano-roughness S_a (nm)	Contact Angle (°)	Phases (XRD)	Phase Content (%)	Bond Strength on Ti64 (MPa)
HA	4.1 ± 0.5	336 ± 5	300 ± 6	102	HA	55	13
					CaP amorphous	44	
					TCP traces	1	
TiO_2	2.2 ± 0.3	63 ± 3	50 ± 4	62	TiO_2 anatase	17	>77
					TiO_2 rutile	83	
TiO_2–HA	3.0 ± 0.5	50 ± 2	50 ± 3	29	TiO_2 anatase	15	>77
					TiO_2 rutile	75	
					HA	10	

(10 mg/mL in 2% BSA/DPBS). Samples were finally mounted in Vectashield (Vector) and examined with a Cell Observer System (Carl Zeiss).

Cell morphology

Cell morphology, spreading, and orientation were evaluated using SEM. Harvested cells were washed twice with PBS and fixed with 1% glutaraldehyde, first for 1 h at room temperature, then overnight at 4°C. The samples were rinsed with PBS for 30 min and then dehydrated through a series of graded alcohol solutions. The specimens were air-dried overnight and the dry cellular constructs were finally sputter coated with palladium and observed under the SEM at an accelerating voltage of 2.0 kV.

RESULTS

Coating characterization

The cross-section of TiO_2–HA coatings EDX line scan analysis (Fig. 1) was performed at the upper layers of TiO_2–HA coating surface to elucidate the dispersed HA crystals chemical interaction with the dominant TiO_2 phase. The EDX analysis identified the presence of micro-regions with co-existence of Ca, P and Ti elements in melted particles, thereby indicating the interdiffusion of elements from HA and TiO_2 in a chemical interaction. The SEM micrographs (Fig. 2) show the surface coating morphology of the pure HA and TiO_2 reference coatings and novel TiO_2–HA coatings. The HA coating is characterized by a smooth surface at the low micron- and nano- scale (higher magnification picture), whereas the TiO_2 coating is characterized by the spherical crystallites at its surface of diameter below 300 nm, as well as the nano-zoned microagreates of TiO_2. On the other hand, the TiO_2–HA coating demonstrates (i) zones of inter-diffusion between the HA and TiO_2 phases as well as (ii) the HA and TiO_2 phases in a distinct fashion. In these distinct regions, the HA particles are represented by the rod-like crystallites shapes 20–30 nm in diameter and 50–100 nm in length (confirmed by EDX) whereas the TiO_2 nano-particles are similar in appearance to the spherical ones observed on the pure TiO_2 coating.

The micro-roughness values of the coatings, as measured by a surface profiler (Table I), do not demonstrate the nano-range differences seen in the SEM images among the coatings. Rather, the surface differences imparted by the HA addition are better demonstrated by the nano-roughness expressed as the linear average (R_a) and 3D surface roughness (S_a) measured by confocal microscopy represented in Figure 3. Compared with the HA coatings, the TiO_2 and the

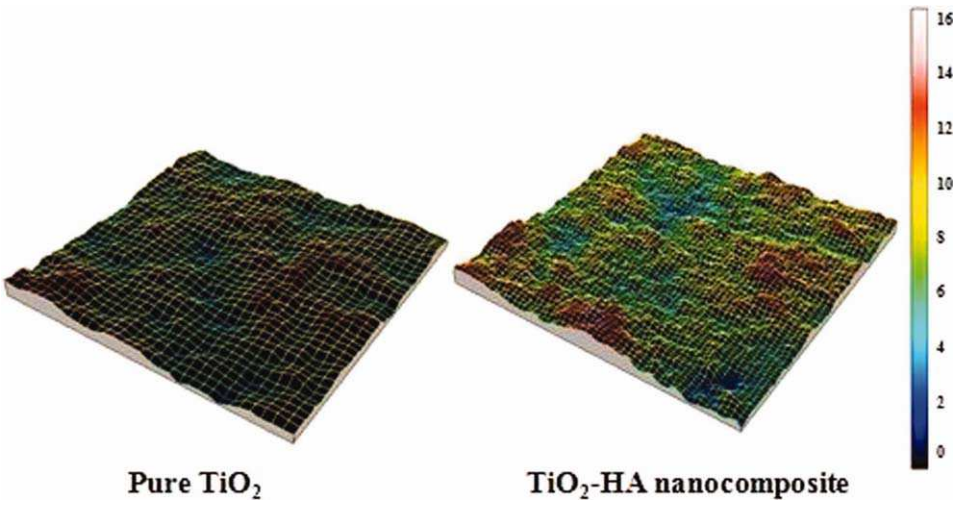

FIGURE 3. Three-dimensional visualizations of the nano-roughness of TiO_2–HA nanocomposite (left) compared with the pure TiO_2 (right). [Color figure can be viewed in the online issue, which is available at wileyonlinelibrary.com.]

TiO_2–HA coatings demonstrate a five and seven times smaller R_a and S_a. This was expected due to the nano-sized character of the coatings as opposed to HA smooth surface especially at the nano level. The smaller R_a value of the TiO_2–HA coatings as compared with that of TiO_2 was probably due to the addition of the HA nanosized rod shaped crystals. The contact angle (Table I) measurements also reflect this nanosized addition with the sharp contact angle decrease (2× smaller for TiO_2–HA), indicating a more hydrophilic surface. The differences among the TiO_2–HA and TiO_2 coatings surface morphologies are visually demonstrated in the confocal images presented in Figure 3 where the smaller R_a of TiO_2–HA is visually compared with TiO_2 and the rougher surface of TiO_2–HA and the nano-level is displayed. Visually this is also reflected in 3D but the measured S_a is not sufficiently sensitive to translate this visual observation into a numeric one.

Cell adhesion and cell growth

To evaluate the initial cell adhesion, the metabolic activity of the cells cultured on the different coatings was measured after 2 and 6 h of culture using Alamar Blue assay [Fig. 4(a)]. Results showed that the adhesion of hMSCs to the TiO_2–HA nanocomposite was improved by 20% after 2 h ($p = 0.02$) compared with both HA and TiO_2 coatings, although this difference remains statistically insignificant. The same trend was also observed after 6 h. However, there were no differences in the adhesion of hMSC-ob on the different coatings at these times.

The proliferation of hMSC and hMSC-ob viability on the various coatings was then also evaluated by Alamar Blue for up to 14 days [Fig. 4(b)]. Results revealed a higher metabolic activity of both hMSC and hMSC-ob on the TiO_2–HA nanocomposite coatings when compared with the pure TiO_2 and HA coatings, at 7 days of culture of 40% ($p = 0.002$) and 30% ($p = 0.01$), respectively. The cell metabolic activity increased on all coatings during the 14-day course, with a five-fold increase for the hMSC and a three-fold increase for the hMSC-ob between day 1 and day 14. These increased metabolic activities correlated with increased protein content at day 14 that reached six and four times the values at day 1 for hMSC and hMSC-ob, respectively.

Osteoblastic markers

Figure 5 shows the levels of two important markers of osteoblast activity,[23,24] ALP and OC, after culture of hMSC and hMSC-ob on the different coatings. Although both markers were expressed on all surfaces in both hMSC and hMSC-ob cultures, significant differences and visible trends among the various coatings were observed. ALP activity reached a peak after 7 days of culture and dropped thereafter [Fig. 5(a)]. At the peak of its activity (7 days), the activity of hMSC and hMSC-ob cultured on the TiO_2–HA nanocomposite coatings was significantly higher than the activity on the HA and TiO_2. As expected, the ALP activity was higher in hMSC-ob than in hMSC after 7 and 21 days in culture on most of the surfaces.

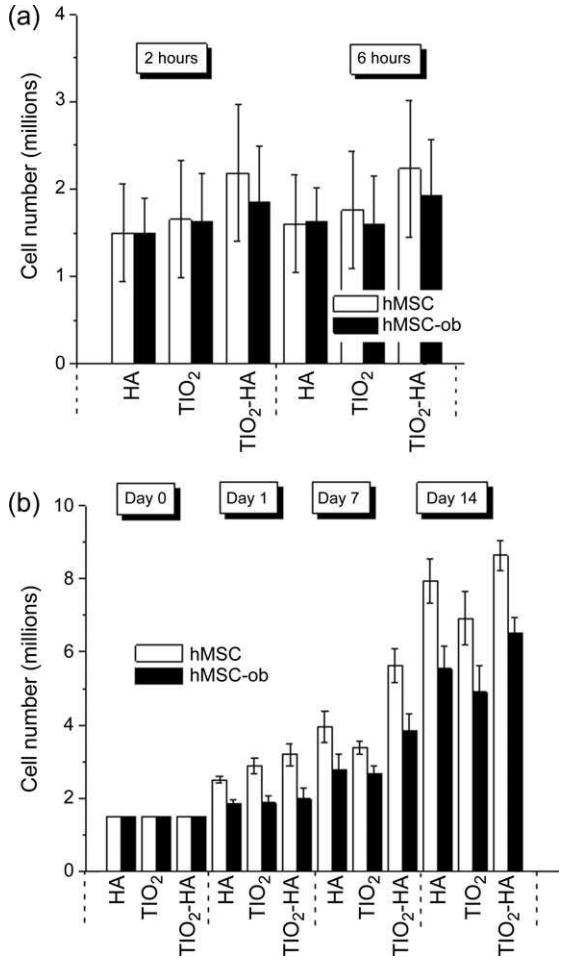

FIGURE 4. Adhesion and proliferation of hMSC and hMSC-ob cultured on nanocomposites. (a) hMSC and hMSC-ob were cultured on the different surfaces for 2 and 6 h to measure the initial adhesion of the cells. (b) hMSC and hMSC-ob were cultured on the different surfaces for up to 14 days on the different surfaces to measure the proliferation of the cells. Metabolic activity was measured by Alamar Blue. Results are expressed as the mean ± SD of three experiments performed in triplicate.

Similarly to what we observed for ALP activity, at the OC expression peak (day 21) the expression was higher on the TiO_2–HA nanocomposite than on the pure HA and TiO_2 coated substrates in hMSC ($p = 0.008$) and hMSC-ob ($p = 0.04$), shown in Figure 5(b). Although there were no significant differences between the hMSC and hMSC-ob cultures for up to 7 days, the expression of OC was significantly higher (1.25 times, $p = 0.0007$) in hMSC-ob than in hMSC plated on the same coatings. The higher ALP activity and OC expression in hMSC-ob supports the success of the osteoblastic differentiation of hMSC in the OC medium.

In vitro mineralization

To determine if the upregulated ALP activity and OC expression correlated with the extracellular matrix mineralization, the mineral deposits were first visualized using calcein stain. As calcein can bind nonspecifically to the HA coating itself, calcein staining was performed after 21 days of cell

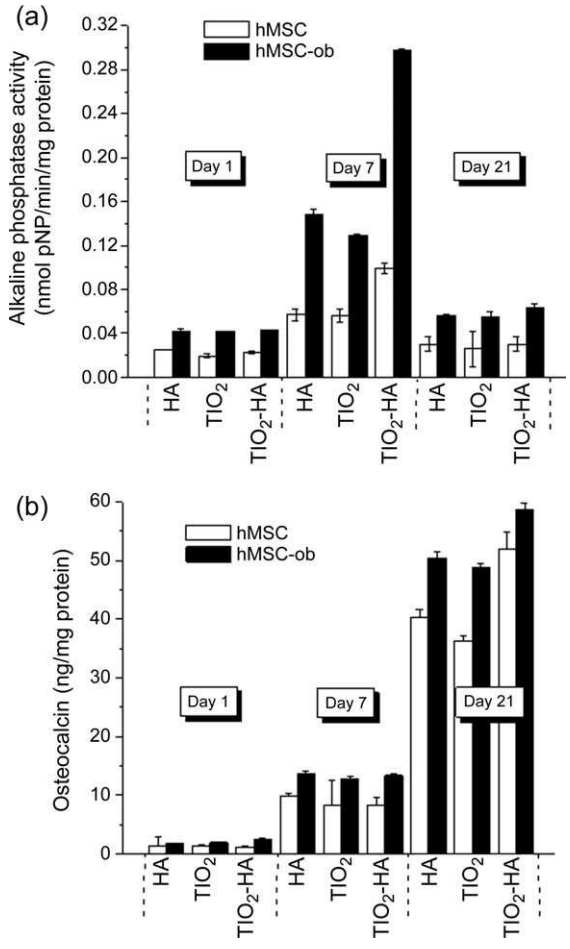

FIGURE 5. Osteoblastic markers in hMSC and hMSC-ob cultured on nanocomposites. Cells were incubated up to 21 days on the different surfaces and alkaline phosphatase (ALP) activity (a) and osteocalcin (OC) expression (b) were measured in cell lysates. Results are expressed as the mean ± SD of three experiments performed in triplicate.

culture, when the coated surfaces are covered by a continuous cell monolayer. In addition, the washing step was improved from the standard literature protocol[21] to further reduce non specific calcein/HA coating interactions. In hMSC cultures, calcein staining was visualized only on the TiO_2–HA nanocomposite coating (Fig. 6). No calcein staining was observed in hMSC cultured on the HA and the TiO_2 substrates. In hMSC-ob cultures, calcein stain was observed on all coatings. The hMSC-ob cultures contained visually denser and more concentrated mineralization nodules.

As a further step in understanding the interaction of hMSC and hMSC-ob with the different coatings, the mineralization process was quantified by ARS (Fig. 7). The ARS results further confirmed the positive effect of TiO_2–HA nanocomposite coating on hMSC osteogenic differentiation. More specifically and as observed for calcein staining (Fig. 6), ARS stain was significantly denser on the hMSC-ob cultured on the TiO_2–HA nanocomposite coatings. The hMSC cultures without osteogenic medium displayed scarce ARS only when cultured on the TiO_2–HA nanocomposite coatings. The quantification of ARS showed nonsignificantly different absorbance values for the hMSC-ob plated on the TiO_2–HA nanocomposite and HA coatings. The hMSC cultures without osteogenic medium demonstrated significantly higher optical density ($p = 0.002$) on the TiO_2–HA nanocomposite coatings when compared with the other coatings.

Cytoskeletal organization, cell–substrate interactions, and cell morphology

Confocal microscopy was used to investigate the distribution of F-actin filaments in hMSC and hMSC-ob cultured on the different surfaces from 1 to 14 days. As shown in Figure 8, the immunostaining of F-actin (green) and the staining of nuclei with PI (red) clearly showed a difference in the phenotype and the growth kinetics between the two types of cells and the different surfaces. At day 1, hMSC [Fig. 8(a)] showed their typical spindle-shaped morphology, similar on all three coatings, with well formed F-actin filaments. By day 7, the F-actin filaments were more intense, denser, and widespread on the TiO_2–HA nanocomposite than on the HA and TiO_2 coatings. Also, the F-actin filaments tended to be generalized over the entire TiO_2–HA nanocomposite surface and not limited only to areas of high cell density. On the other hand, hMSC-ob [Fig. 8(b)] cultured for 1 day on the three coatings demonstrated a generally more polyglonal cell morphology with formation of clusters. No evident differences were observed among the various coatings. Similarly as the hMSC, at day 7 the hMSC-ob demonstrated a much more intense and widespread staining of F-actin filaments on the TiO_2–HA nanocomposite as compared with the HA and TiO_2 surfaces. Again, the hMSC-ob expression was most prominent around cells closely associated with the TiO_2-HA nanocomposites and their growth kinetics seemed to be increased as the number of PI marked nuclei increased.

To further analyze cytoskeleton structure and the degree of cell adhesion of hMSC and hMSC-ob cultured on the different surfaces, immunostaining of F-actin and vinculin was performed at 14 days of culture (Fig. 9). These combined stainings reveal the strength and the extent of molecular interaction (mainly through integrin binding) with the coatings.[10,25] The cells exhibited a diffuse staining of cytoplasmic vinculin that could be attributed to nonspecific staining or over-confluence, as the patchy signals were indicative of focal contacts. The distribution patterns and morphology of focal contacts were notably different among the various coatings and among the type of cells. Particularly, hMSC and hMSC-ob plated on the TiO_2–HA nanocomposites showed the highest density of focal adhesion. In addition, hMSC plated on the TiO_2–HA nanocomposites displayed dense "long" and "short" vinculin-stained focal adhesions, all oriented along the same axis. This differed from the hMSC cultured on HA coatings that showed only randomly oriented "short" vinculin-stained focal adhesions. The vinculin-stained focal adhesion of hMSC-ob demonstrated a higher "short" vinculin density on the TiO_2–HA nanocomposites and TiO_2 coatings. Finally, a distinct lack of contacts for both cell types on the pure HA substrates were observed.

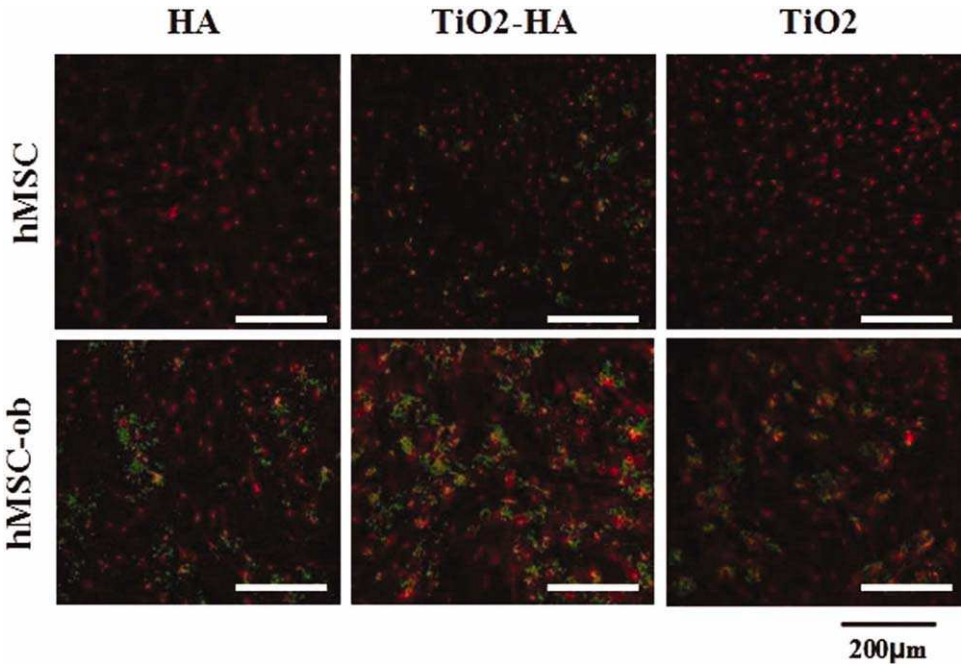

FIGURE 6. Mineralization in hMSC and hMSC-ob cultured on nanocomposites. Cells were incubated for 14 days on HA, TiO_2–HA nanocomposite, and TiO_2 coatings. Cells were then stained with calcein (green) to visualize calcium and with PI (red) to visualize DNA. Original magnification was 200×. [Color figure can be viewed in the online issue, which is available at wileyonlinelibrary.com.]

Cell morphology on the HA and TiO_2–HA nanocomposites and on TiO_2 coatings was also studied using SEM (Fig. 10). Because both hMSC and hMSC-ob cell types had similar morphology on the different coatings, only results with hMSC are presented. After 2 days of culture, hMSC adhered on all coatings, elongated, and took on a typical "shuttle" hMSC shape. However, hMSC cultured on HA coatings appeared less spread and in a more rounded configuration than the hMSC cultured on the TiO_2–HA nanocomposites and TiO_2 coatings. After 7 days of culture the hMSC cultured on the HA coatings flattened and spread with no clear tendency towards a cell monolayer or nodule formation. On the other hand, cells on the TiO_2–HA nanocomposites and the TiO_2 coatings at day 7 showed a cell coverage over the coating surface where the hMSC had proliferated to form a monolayer. Nodule formation was also observed.

DISCUSSION

The superior mechanical performance and micro-topography of HVOF-sprayed TiO_2–HA coatings have been introduced in previous works.[21] In the present study we characterized the nanosurface topography effects of the TiO_2–HA coatings on the surface hydrophilicity and roughness, and the HA nanoshaped crystals chemical interaction with the TiO_2 matrix. We also evaluated the physicochemical surface characteristics effects on the osteogenic differentiation of human bone marrow derived cells, revealing a high *in vitro* osteoinductivity potential supporting them as mechanically and biologically improved load-bearing implant coatings. Indeed, hMSC, the initially recruited cells on orthopaedic load-bearing implants,[7] adhered, expanded, and differentiated into an osteoblast phenotype in a more efficient manner on the TiO_2–HA nanocomposite than on HA coatings. To the authors' knowledge, this is the first work on the interaction of human primary bone marrow derived cells with HVOF-sprayed TiO_2–HA nanocomposite coatings.

More precisely, the present data is in agreement with previous reports with immortalized osteoblastic cell lines[13,14,18] and primary mouse cells[12] cultured on TiO_2–HA coatings where some osteoblast functions were increased on TiO_2–HA coatings when compared with HA-coated Ti substrates.[13] Our results showed an increased adhesion and proliferation of both hMSC and hMSC-ob on this nanocomposite, suggesting that stem cells create a stronger initial adhesion on the TiO_2–HA nanocomposite allowing increased growth kinetics. The structure of the cells, as visualized by F-actin labelling, seem to be more affected by the support coating than the culture conditions (basal unsupplemented medium *vs.* osteogenic medium) used. This strongly suggests that the increased osteoblastic markers are largely dependent on the physicochemical and topographical features of TiO_2–HA nanocomposite, and not only on the differentiation factors added in the culture media.

Although increased cellular proliferation and adhesion is generally desirable for hard-tissue implants, the formation of a fibrous capsule remains a major problem as bone marrow stomal cells also undergo differentiation into soft tissues.[23,26] It is therefore pivotal that the ideal coating not only recruits higher cell numbers and allows increased proliferation, but also possesses the capacity to facilitate differentiation of osteoprogenitors to mature mineral-producing osteoblasts.[7] In this regard, the markers of osteoblastic activity measured in this study, ALP an early marker and OC a late marker, were significantly higher on the TiO_2–HA

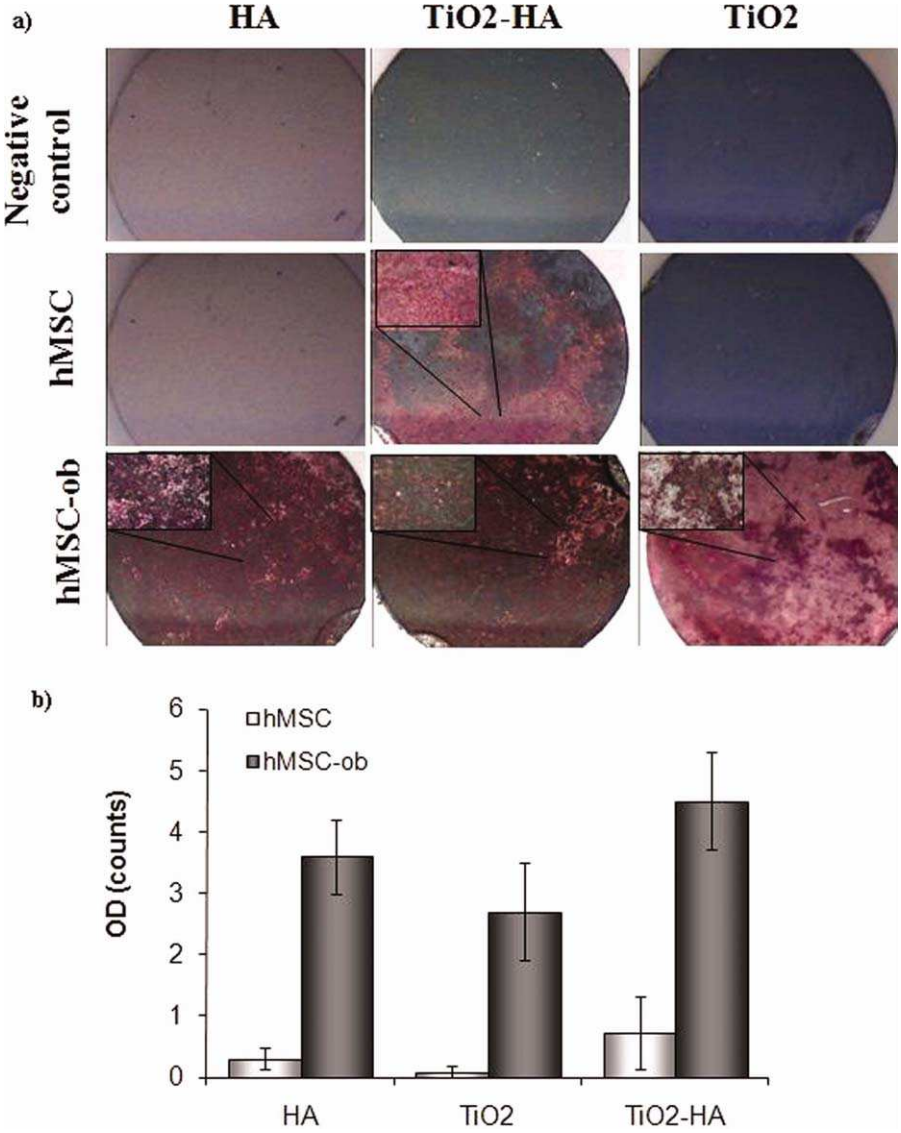

FIGURE 7. Quantification of the mineralization in hMSC and hMSC-ob cultured on nanocomposites. Cells incubated on HA, TiO_2, and TiO_2–HA nanocomposites coatings were stained for alizarin red (ARS) at 14 days of culture (a). The quantification (OD) of the destained ARS is presented in (b). [Color figure can be viewed in the online issue, which is available at wileyonlinelibrary.com.]

nanocomposites than on the HA and TiO_2 reference coatings. In fact, the increase in ALP activity is an indication of the higher commitment toward osteoblastic lineage, whereas the subsequent temporal decrease superimposed with OC increase correlates with advanced matrix mineralization and a more mature phenotype.[26,27] Similar osteogenic properties were also observed for hMSCs cultured on nanotopographical surfaces in which a surface-dependent increase of osteoblastic activity, without the addition of supplemented medium, has been described.[26,28]

The hMSC osteogenic differentiation can be induced through several common tropic factors.[7,11,26] In this study, the differentiation was induced in a simple and inexpensive way using a cocktail of three different drugs in which the key member was dexamethasone. Dexamethasone is necessary for *in vitro* bone nodule formation and mineralization in marrow stroma-derived cell cultures.[29] However the colocalization of alizarin red and calcein stain (markers of calcium deposit) observed in hMSC cultures plated on TiO_2–HA nanocomposites without the addition of external supplements suggested that these cells are already committed to the osteoblastic lineage. This is in agreement with previous characterization works by our group demonstrating the expression of osteoblastic markers[30,31] and type X collagen,[32] a marker of late stage chondrocyte hyperthrophy implicated in ossification, in MSCs from patients with osteoarthritis. It is important to note that these patients are typical candidates for total hip replacement and the coating described in the present study may be beneficial. The mineralization capacity of hMSC on TiO_2–HA nanocomposites in the absence of dexamethasone on the novel TiO_2–HA nanocomposites surface is highly important for the development

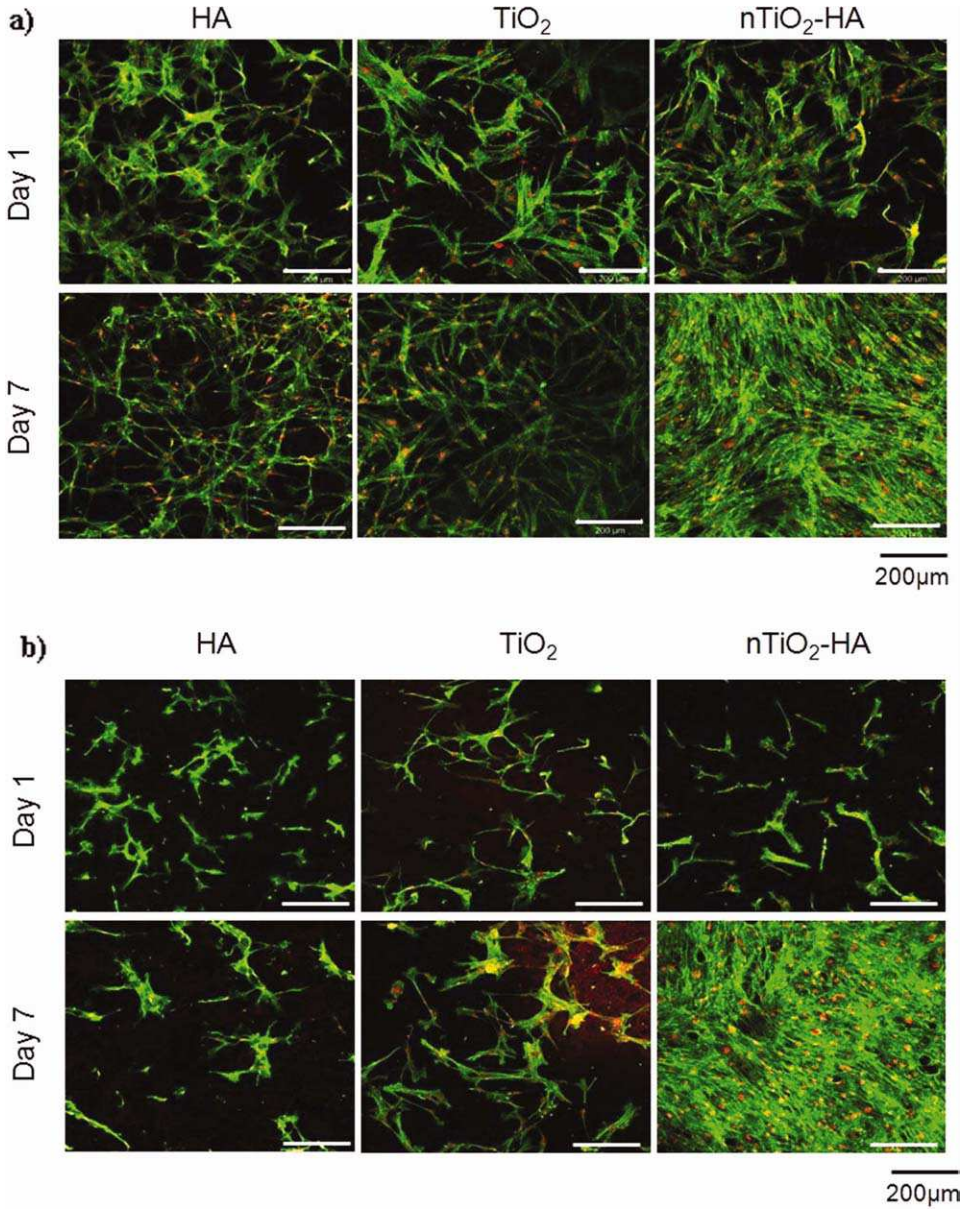

FIGURE 8. Cytoskeleton organization in hMSC and hMSC-ob cultured on nanocomposites. hMSC (a) and hMSC-ob (b) were incubated up to 7 days on HA TiO_2–HA nanocomposites and on TiO_2 coating. F-actin filaments were stained with TRITC-phalloidin (green) and nuclei with PI (red). Original magnification was 200×. [Color figure can be viewed in the online issue, which is available at wileyonlinelibrary.com.]

of bone regeneration coatings. In comparison, hMSC cultured on HA and TiO_2 only mineralized when supplemented with dexamethasone. This is common with many osteoblast cell cultures when the surface is insufficiently inductive,[33] such as seen in literature with bioactive HA and TiO_2–HA coatings expressing biocompatibility towards bone marrow cell lines, yet requiring the addition of differentiation factors for optimal cell responses.[12–14,18] Here, the mineralized nodule formation (alizarin red and calcein stains), increased ALP activity and OC expression, and increased extracellular matrix production (cytoskeletal organization marked by the cell cytoskeletal F-actin) strongly suggest that TiO_2–HA nanocomposite coatings can induce the mineralization process without the addition of any of these factors.

The mechanism underlying the induced osteogenic differentiation of the hMSC on the TiO_2–HA nanocomposites is not well understood yet. The following physical factors probably come into play: (1) the high hydrophilicity and hydroxyl group coverage of the coatings, facilitating the initial cellular adhesion and spreading; (2) the nano-topography (texture) of the surface, increasing the initial protein and cell adhesion; (3) the HA nano-rod shaped crystals, increasing the HA nucleation potential and cell cultures mineralization initiation; (4) the chemical interaction between TiO_2 and HA resulting in additional nucleation sites such as Ti-OH and TiO_2 nanoparticles[33–35] in addition to the micro-regions of Ca, P and Ti interdiffusion sites created from chemical HA and TiO_2 coexistence. The high affinity of

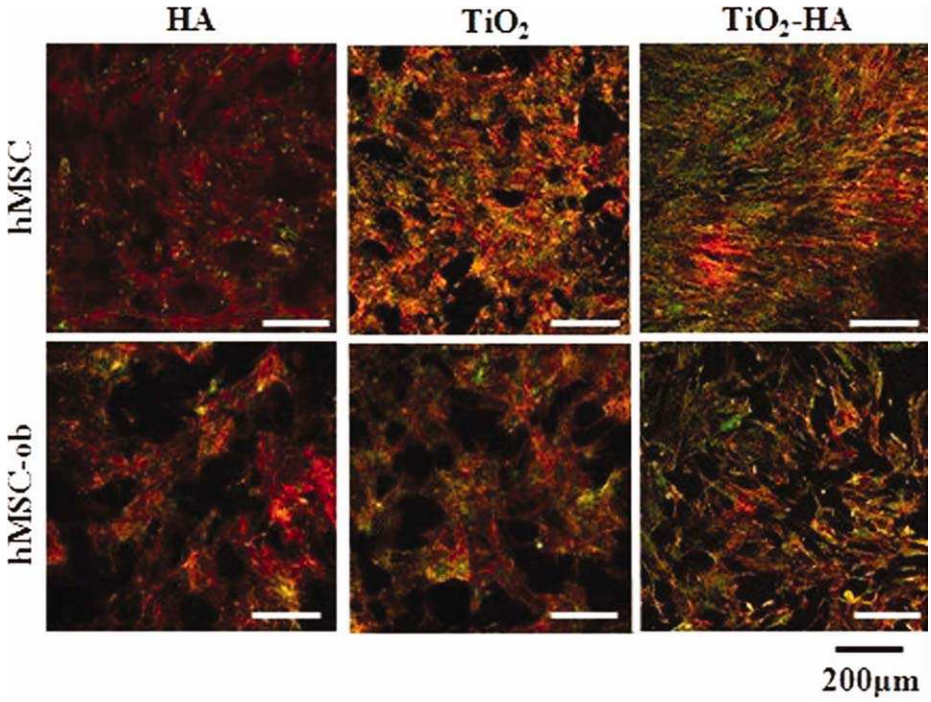

FIGURE 9. Focal adhesion of hMSC and hMSC-ob cultured on nanocomposites. Cells were incubated for 14 days on HA, TiO_2, and TiO_2–HA nanocomposite coatings and then stained for F-actin (red) and vinculin (green) to visualize focal adhesion. Original magnification was 200×. [Color figure can be viewed in the online issue, which is available at wileyonlinelibrary.com.]

TiO_2 nanoparticles towards the absorption of organic groups has been speculated to favour the absorption of serum proteins upon cell seeding and matrix deposition by the cultured cells.[12] As previously shown, TiO_2 coatings initiate the growth of an interface of bonded calcium phosphate (CaP) forming a layer similarly as on CaP-coated materials known to initiate mineralization of rat MSC.[36] This directly bonded layer of about 500 nm facilitates CaP deposits, further supporting mineralization. Also, the presence of hydroxyl groups such as Ti-OH on the TiO_2–HA nanocomposite surface has been shown to provide a site for CaP nucleation.[18] As TiO_2–HA nanocomposites contain both TiO_2 nano-zones (spherical nano-sized crystallites) and HA hydroxyl (OH) species (rod-shaped nano-sized crystallites in addition to flatter micron-sized aggregates), it can be postulated that protein absorption and extracellular matrix formation that readily take place on nano-TiO_2 surfaces would be enhanced by the addition of the OH groups. The ability of nanophases to promote interaction with serum proteins and stimulate osteoblast adhesion[6,37] is also believed to

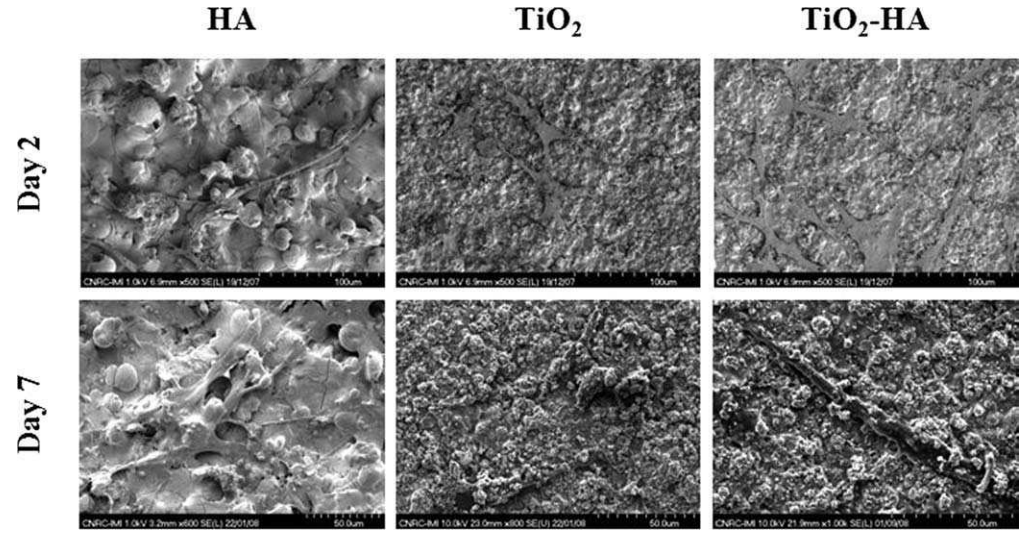

FIGURE 10. Surface morphology of hMSC cultured on nanocomposites. Cells were incubated for 2 and 7 days on HA, TiO_2, and TiO_2–HA nanocomposites and visualized by FEG-SEM. Images were acquired at a 100-μm scale at 2 days and at a 50-μm scale at 7 days.

support hMSC mineralization. This suggests that the nano/sub-micron topography of the TiO_2–HA nanocomposite may be involved in its osteogenic properties. In addition, the reduced nano-roughness (both R_a and S_a) of the samples may also play a role. Indeed, it has been observed that human osteoblasts do not conform well to micro-irregularities of Ti surfaces, suggesting that a lower roughness facilitates human osteoblast adhesion.[3] The TiO_2–HA nanocomposites exhibited far lower roughness and higher hydrophilicity than APS HA coatings which may be attributed to both its chemistry and processing method. Future research work will need to address the possible relationships between the nanotopography and the surface chemistry to better explain the events observed in this research.

CONCLUSION

Results of the present study suggest that the novel HVOF sprayed TiO_2–HA nanocomposite coatings, that exhibit superior mechanical strength and bonding, also demonstrate chemically bound HA to the coatings surface, higher hydrophilicity and a superior mineralization capacity of hMSC in the absence of dexamethasone as seen though mineral nodule formation (alizarin red and calcein stains), increased ALP and OC expression, and increased extracellular matrix production (cytoskeletal F-actin). The mineralization capacity of stem cells on the novel TiO_2–HA nanocomposite surface is highly important for the development of bone regeneration coatings. Taken together, these results indicate that the TiO_2–HA nanocomposites coatings, in addition to being easily transferable to clinical settings, also have a high osteoinductivity, which supports them as potential mechanically and biologically improved load-bearing implant coatings.

REFERENCES

1. Bianco P, Robey PG. Stem cells in tissue engineering. Nature 2001;414:118–121.
2. Dalby MJ, Gadegaard N, Tare R, Andar A, Riehle MO, Herzyk P, Wilkinson CD, Oreffo RO. The control of human mesenchymal cell differentiation using nanoscale symmetry and disorder. Nat Mater 2007;6:997–1003.
3. Lima RS, Marple BR. Thermal spray coatings engineered from nanostructured ceramic agglomerated powders for structural, thermal barrier and biomedical applications: A review. J Therm Spray Tech 2007;16:40–63.
4. Gaona M, Lima RS, Marple BR. Nanostructured titania/hydroxyapatite composite coatings deposited by high velocity oxy-Fuel (HVOF) spraying J Mater Sci Eng A 2007;458:141–149.
5. Cecil RH. Tapered hydroxyapatite-coated press-fit stems: Any added value? J Arthroplasty 2006;21:85–88.
6. Chen F, Lam WM, Lin CJ, Qiu GX, Wu ZH, Luk KD, Lu WW. Biocompatibility of electrophoretical deposition of nanostructured hydroxyapatite coating on roughen titanium surface: in vitro evaluation using mesenchymal stem cells. J Biomed Mater Res B Appl Biomater 2007;82:183–191.
7. Dalby MJ, McCloy D, Robertson M, Wilkinson CD, Oreffo RO. Osteoprogenitor response to defined topographies with nanoscale depths. Biomaterials 2006;27:1306–1315.
8. Curran JM, Chen R, Hunt JA. The guidance of human mesenchymal stem cell differentiation in vitro by controlled modifications to the cell substrate. Biomaterials 2006;27:4783–4793.
9. Lee JY, Choo JE, Choi YS, Park JB, Min DS, Lee SJ, Rhyu HK, Jo IH, Chung CP, Park YJ. Assembly of collagen-binding peptide with collagen as a bioactive scaffold for osteogenesis in vitro and in vivo. Biomaterials 2007;28:4257–4267.
10. Richardson SM, Curran JM, Chen R, Vaughan-Thomas A, Hunt JA, Freemonta AJ, Hoyland JA. The differentiation of bone marrow mesenchymal stem cells into chondrocyte-like cells on poly-L-lactic acid (PLLA) scaffolds. Biomaterials 2006;27:4069–4078.
11. Xin X, Hussain M, Mao JJ. Continuing differentiation of human mesenchymal stem cells and induced chondrogenic and osteogenic lineages in electrospun PLGA nanofiber scaffold. Biomaterials 2007;28:316–325.
12. Carbone R, Marangi I, Zanardi A, Giorgetti L, Chierici E, Berlanda G, Podestà A, Fiorentini F, Bongiorno G, Piseri P, Pelicci PG, Milani P. Biocompatibility of cluster-assembled nanostructured TiO_2 with primary and cancer cells. Biomaterials 2006;27:3221–3229.
13. Sato M, Aslani A, Sambito MA, Kalkhoran NM, Slamovich EB, Webster TJ. Nanocrystalline hydroxyapatite/titania coatings on titanium improves osteoblast adhesion. J Biomed Mater Res A 2008;84:265–272.
14. Kim HW, Kim HE, Salih V, Knowles JC. Hydroxyapatite and titania sol-gel composite coatings on titanium for hard tissue implants; mechanical and in vitro biological performance. J Biomed Mater Res B Appl Biomater 2005;15:1–8.
15. Xuanyong L, Xiaobing Z, Ricky KY, Joan PY, Chuanxian D, Paul KC. Plasma-treated nanostructured TiO_2 surface supporting biomimetic growth of apatite. Biomaterials 2005;26:6143–6150.
16. Lee SH, Kim HW, Lee EJ, Li LH, Kim HE. Hydroxyapatite-TiO_2 hybrid coating on Ti implants. J Biomater Appl 2006;20:195–208.
17. Zheng XB, Ding CX. Characterization of plasma-sprayed hydroxyapatite/TiO_2 composite coatings. J Therm Spray Technol 2000;9:520–525.
18. Ramires PA, Romito A, Cosentino F, Milella E. The influence of titania/hydroxyapatite composite coatings on in vitro osteoblasts behaviour. Biomaterials 2001;22:1467–1474.
19. Legoux JG, Chellat F, Lima RS, Marple BR, Bureau MN, Shen H, Candeliere GA. Development of osteoblast colonies on new bioactive coatings. J Therm Spray Technol 2006;15:628–633.
20. Auclair-Daigle C, Bureau NM, Legoux JG, Yahia LH. Bioactive hydroxyapatite coatings on polymer composites for orthopedic implants. J Biomed Mater Res A 2005;73:398–408.
21. Bosetti M, Lloyd AW, Santin M, Denyer SP, Cannas M. Effects of phosphatidylserine coatings on titanium on inflammatory cells and cell-induced mineralisation in vitro. Biomaterials 2005;26:7572–7578.
22. Nelea V, Luo L, Demers CN, Antoniou J, Petit A, Lerouge S, Wertheimer MR, Mwale F. Selective inhibition of type X collagen expression in human mesenchymal stem cell differentiation on polymer substrates surface-modified by glow discharge plasma. J Biomed Mater Res A 2005;75:216–223.
23. Dimitrievska S, Whitfield J, Hacking SA, Bureau MN. Novel carbon fiber composite for hip replacement with improved in vitro and in vivo osseointegration. J Biomed Mater Res A 2009;91:37–51.
24. Collin P, Nefussi JF, Wetterwald A, Nicolas V, Boy-Lefevre M, Fleisch H, Forest N. Expression of collagen, osteocalcin, and bone alkaline phosphatase in a mineralizing rat osteoblastic cell culture. Calcif Tissue Int 1992;50:175–183.
25. Diener A, Nebe B, Lüthen F, Becker P, Beck U, Neumann HG, Rychly J. Control of focal adhesion dynamics by material surface characteristics. Biomaterials 2005;26:383–392.
26. Donzelli E, Salvadè A, Mimo P, Viganò M, Morrone M, Papagna R, Carini F, Zaopo A, Miloso M, Baldoni M, Tredici G. Mesenchymal stem cells cultured on a collagen scaffold: In vitro osteogenic differentiation. Arch Oral Biol 2007;52:64–73.
27. Van der Wal E, Vredenberg AM, Ter Brugge PJ, Wolke JG, Jansen JA. The in vitro behavior of as-prepared and pre-immersed RF-sputtered calcium phosphate thin films in a rat bone marrow cell model. Biomaterials 2006;27:1333–1340.
28. Dalby MJ, Gadegaard N, Tare R, Andar A, Riehle MO, Herzyk P, Wilkinson CD, Oreffo RO. The control of human mesenchymal cell differentiation using nanoscale symmetry and disorder. Nat Mater 2007;6:997–1003.

29. Jaiswal N, Haynesworth SE, Caplan AI, Bruder SP. Osteogenic differentiation of purified, culture-expanded human mesenchymal stem cells in vitro. J Cell Biochem 1997;64:295–312.
30. Mwale F, Wang HT, Nelea V, Luo L, Antoniou J, Wertheimer MR. The effect of glow discharge plasma surface modification of polymers on the osteogenic differentiation of committed human mesenchymal stem cells. Biomaterials 2006;27:2258–2264.
31. Mwale F, Girard-Lauriault PL, Wang HT, Lerouge S, Antoniou J, Wertheimer MR. Suppression of hypertrophy and osteogenesis in committed human mesenchymal stem cells cultured on novel nitrogen-plasma polymer coatings. Tissue Eng 2006;12:2639–2647.
32. Mwale F, Stachura D, Roughley P, Antoniou J. Limitations of using aggrecan and type X collagen as markers of chondrogenesis in mesenchymal stem cell differentiation. J Orthop Res 2006; 24:1791–1798.
33. Gough JE, Jones JR, Hench LL. Nodule formation and mineralisation of human primary osteoblasts cultured on a porous bioactive glass scaffold. Biomaterials 2004;25:2039–2046.
34. Liu X, Zhao X, Li B, Cao C, Dong Y, Ding C, Chu PK. UV-irradiation-induced bioactivity on TiO_2 coatings with nanostructural surface. Acta Biomaterialia 2008;4:544–552.
35. Kotobuki N, Ioku K, Kawagoe D, Fujimori H, Goto S, Ohgushi H. Observation of osteogenic differentiation cascade of living mesenchymal stem cells on transparent hydroxyapatite ceramics. Biomaterials 2005;7:779–785.
36. Bruder SP, Kurth AA, Shea M, Hayes WC, Jaiswal N, Kadiyala S. Bone regeneration by implantation of purified, culture-expanded human mesenchymal stem cells. J Orthop Res 1998;16:155–162.
37. Webster TJ, Siegel TW, Bizios R. Osteoblast adhesion on nanophase ceramics. Biomaterials 1999;20:1221–1227.